Index for Simultaneous Dispersive and Distributive Mixing Characterization in Processing Equipment

Article *in* International Polymer Processing · December 2004

DOI: 10.3139/217.1843

CITATIONS
14

READS
731

3 authors, including:

Ica Manas
Case Western Reserve University
139 PUBLICATIONS **3,880** CITATIONS
SEE PROFILE

Miron Kaufman
Cleveland State University
173 PUBLICATIONS **2,592** CITATIONS
SEE PROFILE

K. Alemaskin[1], *I. Manas–Zloczower*[1]*, *M. Kaufman*

[1] *Department of Macromolecular Science, Case Western Reserve University, Cleveland, OH, USA*
[2] *Physics Department, Cleveland State University, Cleveland, OH, USA*

Index for Simultaneous Dispersive and Distributive Mixing Characterization in Processing Equipment

Computer simulation of agglomerate dispersion and sequential distribution of all particles obtained in the system allows us to evaluate the overall mixing efficiency of processing equipment. Evaluation was based on a specific mixing index, calculated using the Shannon entropies for different size fractions. The index can be tailored to give preference to different particle size distributions, thus relating the quality of mixing to specific properties of the final product.

1 Introduction

In polymer processing operations the quality of the final product is highly dependent on mixing. A significant number of theoretical and experimental efforts were undertaken to predict mixing quality dependence on material parameters, design, and processing conditions.

When mixing two immiscible fluids or solid agglomerates within a fluid, a first step is the reduction in size of the minor fluid droplets or the solid clusters in the matrix/major fluid. This process is referred to as dispersive mixing and the criterion to be used in assessing mixing quality should be related to the minor component size distribution. A second step in obtaining a homogeneous mixture is to spread the minor component throughout the matrix. This step is referred to as distributive mixing and the criterion to be employed in judging mixing quality should be related to the spatial distribution of the minor component.

Conventionally processing equipment has been assessed separately for its dispersive and distributive mixing efficiency. Similarly, the final product has been judged separately for its dispersive and distributive mixing quality.

Dispersive mixing performance is generally assessed in terms of specific characteristics of the flow field. *Manas–Zloczower* and *Tadmor* [1] looked at the distribution of the number of passes over the flights in a single screw extruder (regions of high shear stress), as a way to assess distributive mixing performance. *Cheng* and *Manas–Zloczower* [2] used the relative strength of elongational flow components and shear stress distributions in the equipment to characterize dispersive mixing performance. Several researchers [3 to 7] have adopted the same criteria of flow strength (sometimes labeled as the flow number) and/or shear stress distribution [8] to evaluate dispersive mixing. The local and total dispersive mixing performance were analyzed numerically using also two indices, namely the relative strength of elongational flow components and the number of passage distribution [9].

In order to assess the spatial distribution of the minor component, gross uniformity and the intensity of segregation [10] are traditional tools for distributive mixing characterization. *Galaktionov* et al. [11] employed a mapping approach to study distributive mixing in Kenics static mixers and made use of a flux-weighed, slice-averaged, discrete intensity of segregation to characterize mixing in continuous equipment in contrast to the previously used area or volume weighed measures for the intensity of segregation used in 2D or 3D closed prototype flows [12, 13]. A mixing measure employed to illustrate the mixture structure and point out to unmixed regions is the scale of segregation, originally suggested by Danckwerts [14].

Researchers have used various statistical tools to characterize distributive mixing. Among them, pairwise correlation functions [15], the coefficient of variation (a normalized measure of the standard deviation) [16], the standard deviation sigma and the maximum error among average concentrations of finite-sized samples [17]. Recently Renyi entropies have been used as rigorous measures of various aspects of distributive mixing [18, 19].

Tzoganakis and co-authors [20, 21] measured experimentally distributive mixing in twin screw extruders by employing a mixing limited interfacial reaction between polymer tracers. Mixing characterization remains a very complex problem and has to be tailored to the specific application. In fact *Ottino* [22] has stated that appropriate mixing indexes have to be selected in accordance to the problem at hand. In this work we present a new approach to allow for a *simultaneous* characterization of *dispersive* and *distributive* mixing taking place in a single screw extruder. We express the extruder performance in terms of an overall index for mixing efficiency and apply this index to compare the performance of extruders with different designs under different processing conditions using both Newtonian and shear-thinning fluid characteristics.

* Mail address: Manas-Zloczower, Dep. of Macromolecular Science, Case Western Reserve University, 2100 Adelbert Road, Cleveland, OH 44106, USA
E-mail: ■

IPP_ipp_2004_04_1843 – 17.12.04/druckhaus

2 Entropic Mixing Characterization

2.1 Shannon Entropy as a Dynamic Measure of Distributive Mixing

Shannon entropy [23] is defined in terms of the probabilities p_j of M possible outcomes:

$$S = -\sum_{j=1}^{M} p_j \ln p_j. \tag{1}$$

Eq. 1 is the unique representation of the entropy, up to multiplicative positive constant, if S is to satisfy the following requirements: the lowest entropy (S = 0) corresponds to one of the p's being 1 and the rest being zero; the largest value for the entropy is achieved when all p's are equal; and S is additive over partitions of the outcomes.

If we concentrate only on distributive mixing, we divide the space of interest in M equal volume bins and then estimate each probability p_j by the particle concentration in bin #j. The worst distributive mixing in the system (when all particles are in one bin) is characterized by S = 0 and the best mixing (all bins contain equal number of particles) is characterized by the maximum entropy S = ln(M). The number of bins is an important parameter as it determines at what scale of segregation we are evaluating the quality of mixing.

2.2 Entropy of Different Species Present in the System

If the mixing process involves particles of different species (characterized for example by size) the outcomes are determined not only by the spatial distribution (i. e. position of the particles in space) but also by the particle properties (such as particle size). We then rewrite Eq. 1 as:

$$S = -\sum_{c=1}^{C}\sum_{j=1}^{M} p_{c,j} \ln p_{c,j}. \tag{2}$$

Here the index c labels the particle species, the index j labels the spatial bin and $p_{c,j}$ is the joint probability to find a particle of species c in bin j. C is the total number of species present in the system and M is the number of spatial bins. According to Bayes' theorem, the joint probability for a particle to be located in bin j and to be of species c is given by

$$p_{c,j} = p_{j/c} p_c, \tag{3}$$

where $p_{j/c}$ is the probability of finding a particle in bin j conditional on being of species c, and p_c is the probability for species c (irrespective of location). By substituting Eq. 3 into Eq. 2 we obtain:

$$S = -\sum_{c=1}^{C}\sum_{j=1}^{M} \left[\left(p_{j/c} p_c\right) \ln\left(p_{j/c} p_c\right)\right], \tag{4}$$

and following

$$S = -\sum_{c=1}^{C} p_c \sum_{j=1}^{M} \left[p_{j/c} \ln p_{j/c}\right] - \sum_{c=1}^{C} \left[p_c \ln p_c\right] \sum_{j=1}^{M} p_{j/c}. \tag{5}$$

Since $\sum_{j=1}^{M} p_{j/c} = 1$, the Eq. 5 reduces to:

$$S = -\sum_{c=1}^{C} p_c \sum_{j=1}^{M} \left[p_{j/c} \ln p_{j/c}\right] - \sum_{c=1}^{C} \left[p_c \ln p_c\right]. \tag{6}$$

Eq. 6 can be compacted as follows:

$$S = S_{species}(\text{location}) + S(\text{species}), \tag{7}$$

where:

$$S_{species}(\text{location}) = \sum_{c=1}^{C} p_c S_c(\text{location}), \tag{8}$$

$$S_c(\text{location}) \equiv -\sum_{j=1}^{M} \left[p_{j/c} \ln p_{j/c}\right], \tag{9}$$

$$S(\text{species}) \equiv -\sum_{c=1}^{C} \left[p_c \ln p_c\right]. \tag{10}$$

The first term in the right hand side of Eq. 7, $S_{species}$(location), is the entropy associated with particle locations conditional on species and averaged over all species. Since S_c(location) = ln(M), we divide this entropy by ln(M) to get a relative entropy which takes values between 0 and 1. In the following discussion we will use $S_{species}$(location) to characterize the mixing of eroding particles, and measure the quality of distributive mixing of each species (based on the particle size). We then will develop an index that characterizes simultaneously the spatial mixing of each species and a material property, as reflected in a preference for a certain size particles. This index is based on replacing in Eq. 8 the p_c's with Gaussian distribution weights centered on the preferred size.

3 Procedures

3.1 3D Flow Simulation of a Single Screw Extruder

A fluid dynamics package FIDAP was used to simulate the three-dimensional, isothermal, steady flow in four pitch lengths bc single screw extruder. No slip boundary conditions on the solid surfaces were applied. The operating condition of the screw rotation corresponds to 180 min^{-1}.

The finite element mesh of the extruder was composed of 12 288 quadrilateral elements, giving a total number of nodes of 15 124. Fig. 1 shows the finite element mesh for the extruder. We used the following physical parameters of the extruder: barrel diameter D_b = 5 cm, diameter of the screw root D_s = 2.8 cm, clearance distance δf = 0.02 cm, flight thickness e = 0.2 cm.

We studied the influence of the throttle ratio (pressure flow to drag flow) Q_p/Q_d on the extruder performance. Two cases were considered: pure drag flow ($Q_p/Q_d = 0$) and flow with back pressure such that $Q_p/Q_d = -1/2$. Also to analyze the influence of the extruder design on mixing performance, we performed the simulation for three different extruders with helix angles θ_b = 10, 17, and 24 degree. The pitch distance of the extruder L_s was adjusted accordingly to be 2.8 cm, 4.8 cm, and 7.0 cm.

Simulations were performed for a Newtonian fluid of viscosity 1160 Pa·s and a power law model fluid with a Newtonian plateau:

$$\underline{\underline{\tau}} = \begin{cases} \eta_0 \underline{\underline{\dot{\gamma}}} & \text{if} \quad |\dot{\gamma}| \le \dot{\gamma}_0, \\ m|\dot{\gamma}|^{n-1} & \text{if} \quad |\dot{\gamma}| \ge \dot{\gamma}_0. \end{cases}$$

The parameters of the power law model were chosen to match the rheological behavior of low density polyethylene melt with a power law index n = 0.59, a consistency index m = 4680, and the shear rate for the onset of shear thinning $\dot{\gamma}_0 = 30\ s^{-1}$.

3.2 Particle Tracking

Particle tracking allows us to observe the motion of particle tracers within a flow field. The particles are considered to be massless points so that their presence in the system does not affect the flow field or the motion of other particles. We also neglect inertia and gravity forces.

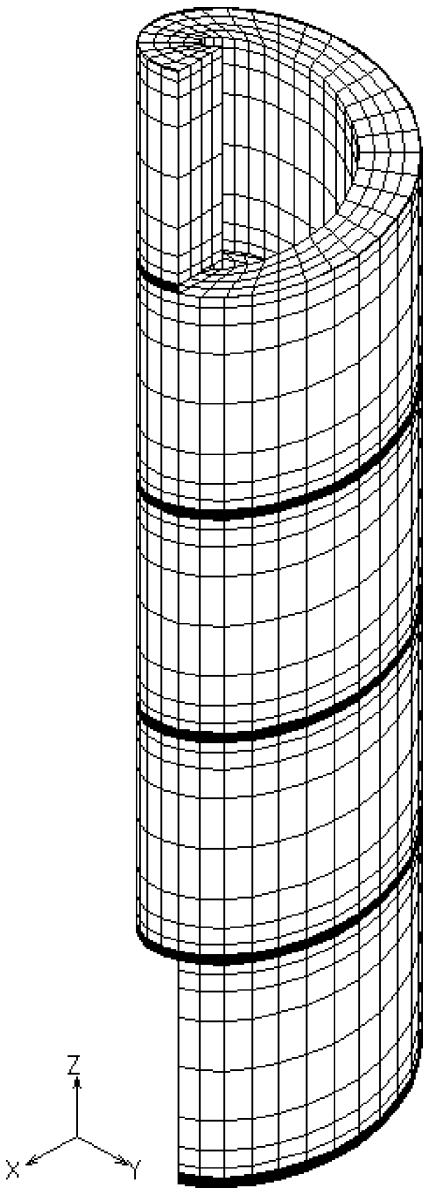

Fig. 1. The finite element mesh for s single screw extruder

The position of a particle at any specific time t can be found by integrating the velocity vector in the flow filed:

$$\underline{X}(t_1) = \underline{X}(t_0) + \int_{t_0}^{t_1} \underline{V}(t)\, dt, \tag{11}$$

where $\underline{X}(t_1)$ is the location of a particle at any time t_1, $\underline{X}(t_0)$ is the location of the particle at the initial time t_0 and $\underline{V}(t)$ is the corresponding velocity vector of the particle. The equation is solved by a Runge-Kutta fourth order integration algorithm [24].

3.3 Dispersive mixing kinetic model

To account for dispersive mixing taking place in the system, particles were considered to be agglomerates of a minor component, allowed to disperse by hydrodynamic forces along their trajectories according to a kinetic model of erosion [25]. In this model the rate of erosion is considered to be proportional to the excess of hydrodynamic force acting on the particle relative to its cohesive force and to the rate at which specific surface positions of the particle experience conditions favorable for erosion. For a simple shear flow the erosion rate can be calculated as

$$-\frac{dR}{dt} = K(F_h - F_c)\frac{\dot{\gamma}}{2}, \tag{12}$$

where R is the agglomerate radius, F_h is the hydrodynamic force acting on it, F_c is the cohesive force resisting dispersion, and $\dot{\gamma}/2$ is the agglomerate rotational speed (with $\dot{\gamma}$ the shear rate). The constant of proportionality K is a parameter specific for a particular system fluid/particle material and can be determined experimentally.

This erosion kinetic model implemented in the particle tracking algorithm does not account for breakage/rupture of initial agglomerates into large fragments.

4 Results and Discussion

We first employ entropy to characterize distributive mixing of 9300 particles along the extruder length. An example of particle spatial distributions at various cross sections along the extruder length is shown in Fig. 2. We assume continuous feeding of particles at the extruder entrance and thus steady-state conditions for all the results presented in this work. Shannon entropies (normalized values), which have been calculated based on such distributions along the extruder length are presented in Fig. 3. A change in helix angle shows little effect on distributive mixing.

To study dispersive mixing in the system we now introduce 100 agglomerates at the entrance plane to the extruder. These agglomerates are exposed to hydrodynamic forces as they travel along the extruder length and consequently will erode according to Eq. 12. During erosion we assumed that parent ag-

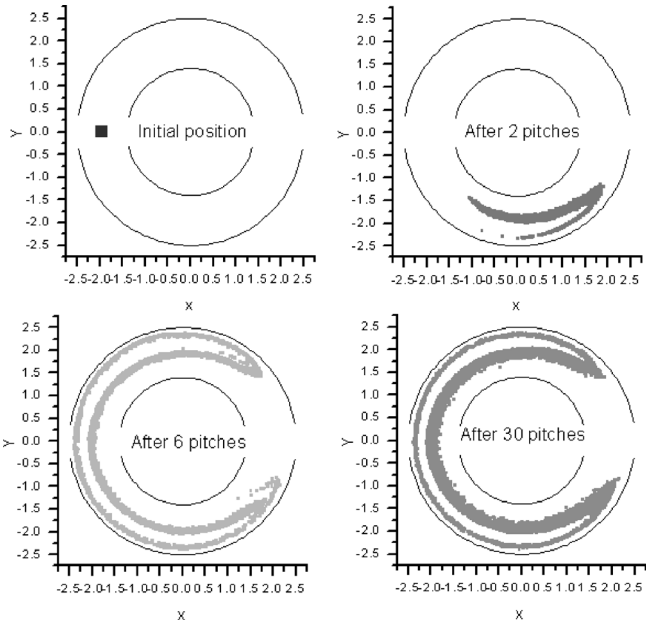

Fig. 2. Particle spatial distributions at different cross sections along the extruder length

glomerates and eroded fragments maintain a spherical shape. The initial agglomerate radius was set at 0.5 mm, while the radius of the smallest eroding fragment was set at 0.11 mm. A simple mass balance shows a maximum of 93 particles to be generated from a single agglomerate thus rendering a maximum of 9300 possible fragments obtained during erosion.

Fig. 4 illustrate the erosion kinetics for the extruders of different designs at two processing conditions for the Newtonian fluid. Reducing the helix angle and operating the extruder at negative throttle ratios seems beneficial. This result can be explained primarily in light of an increasing residence time in the extruder when decreasing the helix angle and operating at negative throttle ratios. A negative throttle ratio will also positively affect the shear rate/stress distribution in the system and consequently enhance dispersion kinetics. Also, by changing the fluid in the system to one exhibiting a shear thinning behavior while maintaining all other properties unchanged (thus allowing the use of the same dispersion kinetic model), erosion is impeded (Fig. 5A and B).

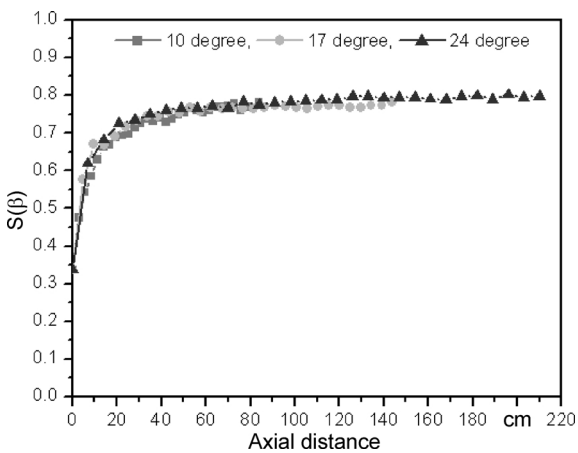

Fig. 3. Evolution of Renyi entropy along the extruder length for Newtonian fluid, 3 rps, $Q_p/Q_d = -0.5$

Referring back to Eq. 9, we can now asses not only the spatial distribution of all particles present in the system, but we also can look at the quality of distribution for a specific particle

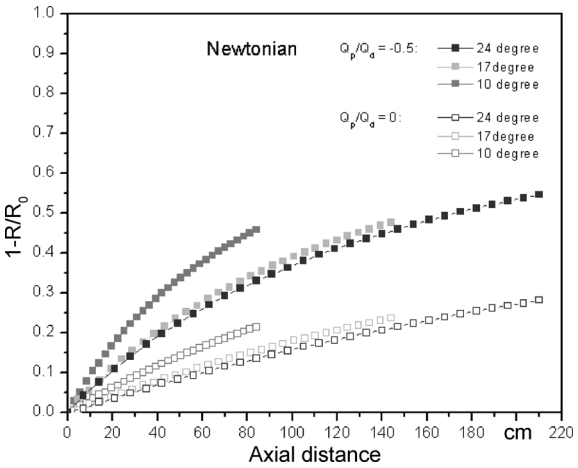

Fig. 4. Erosion kinetics for Newtonian fluid

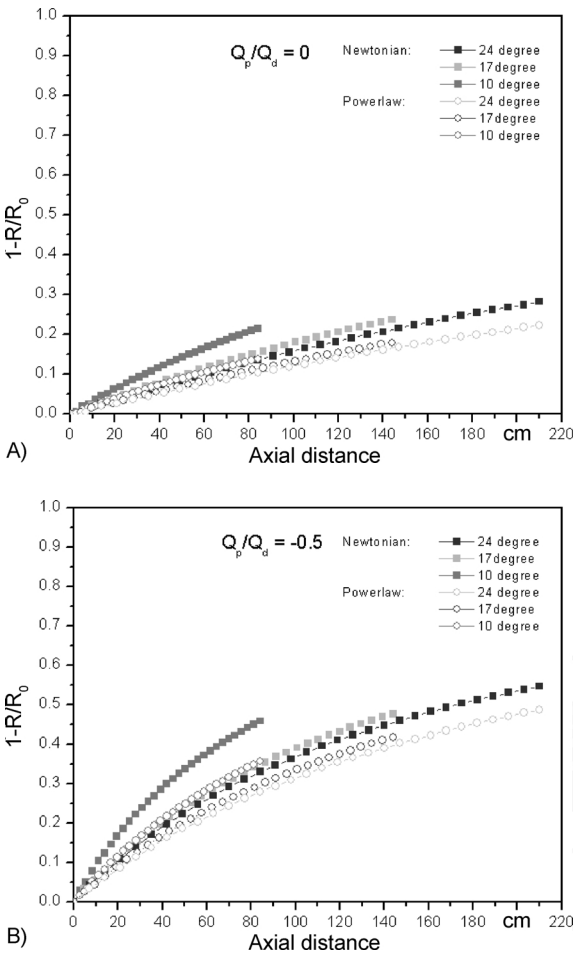

Fig. 5. Comparison of the erosion kinetics for Newtonian and power law fluids, A: $Q_p/Q_d = 0$, B: $Q_p/Q_d = -0.5$

IPP_ipp_2004_04_1843 – 17.12.04/druckhaus

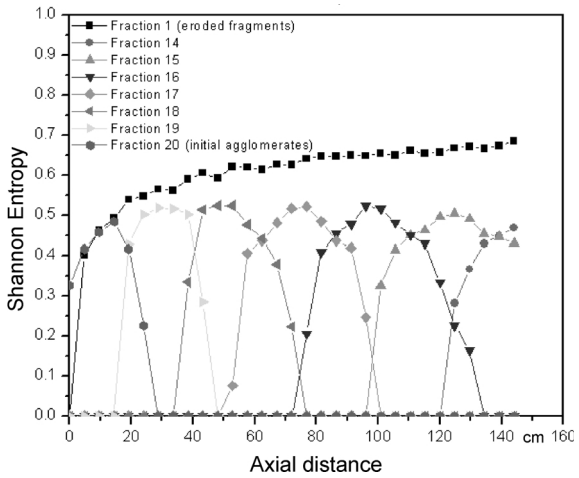

Fig. 6. Evolution of Shannon entropy along the extruder length, 17°, $Q_p/Q_d = 0$

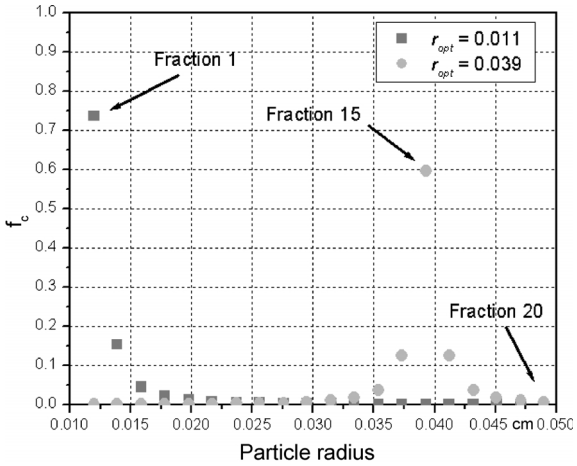

Fig. 8. Weight factors for different size fractions (based on 20 size fractions between the smallest and the largest sizes)

population. These populations are created based on particle physical dimension (radius) as a result of the erosion process.

Fig. 6 shows the evolution of the Shannon entropies associated with the different size species, S_c(location) c = $1 \cdots 20$, for a particular extruder design and processing conditions. The plot starts with a low value of entropy for the largest size fraction (fraction 20) present in the system (initial agglomerates). As these particles advance along the extruder length they get distributed and thus their entropic value increases. However as another fraction (fraction 19) appears in the system, fraction 20 is attrite and consequently its entropic value decreases. Similar behavior is observed for all intermediate species generated in the system as a result of erosion. The ultimate particle size (fraction 1) is constantly accumulated in the system and as particles of these species continue to distribute, entropic value for this size fraction shows a constant growth.

At a given scale of segregation, the entropic value, which characterizes the distribution of the specific population, will be highly dependent on the concentration of particular species in the system. If the number of bins chosen to characterize our

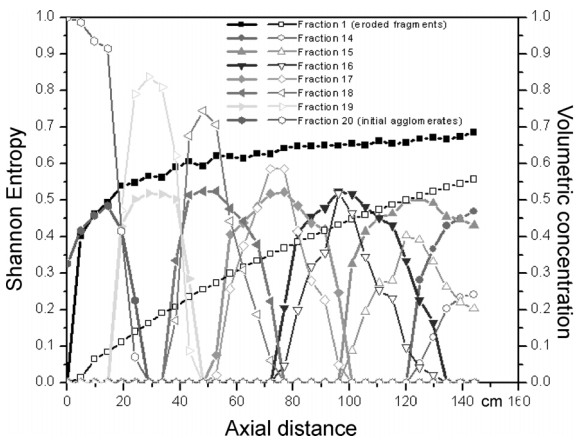

Fig. 7. Evolution of entropy and population distribution along the extruder length, 17°, $Q_p/Q_d = 0$

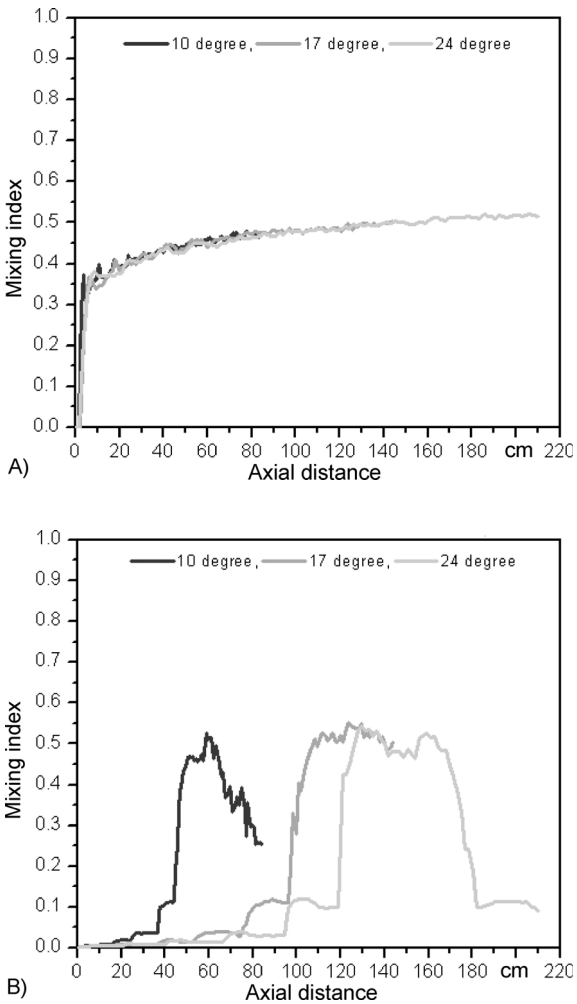

Fig. 9. Evolution of the mixing index in the case of Newtonian fluid along the extruder length when operating the extruder at zero throttle ratio, $Q_p/Q_d = 0$, A: preferred size: 0.011 (smallest), B: preferred size: 0.039 (intermediate)

IPP_ipp_2004_04_1843 – 17.12.04/druckhaus

system is high enough to account for the maximum number of particles to be generated in the system (e. g. 9300 particles in our study), at low concentration of a certain fraction, its entropy is low regardless how well particles of this fraction are distributed. To illustrate this point, in Fig. 7 we superimpose the plot for the entropies and the plot reflecting the change in particle population balance. We can distinguish a good correlation between the loci of maxima in both entropy and concentration, except for the initial size agglomerates.

The entropy of species describes the distribution for particles of that particular size only. However, for practical purposes it is important to evaluate the quality of distributive mixing for different size particles. Furthermore, optical or mechanical properties of the final product dictate which size particles are more important. Consequently, based on $S_{species}$(location), we define an index that is a weighted average of the entropies associated with different species, with weights f_c which reflect the relative importance of different sizes for the physical specifications of the final product:

$$I = \frac{1}{\ln(M)} \sum_{c=1}^{C} f_c S_c(\text{locations}). \tag{12}$$

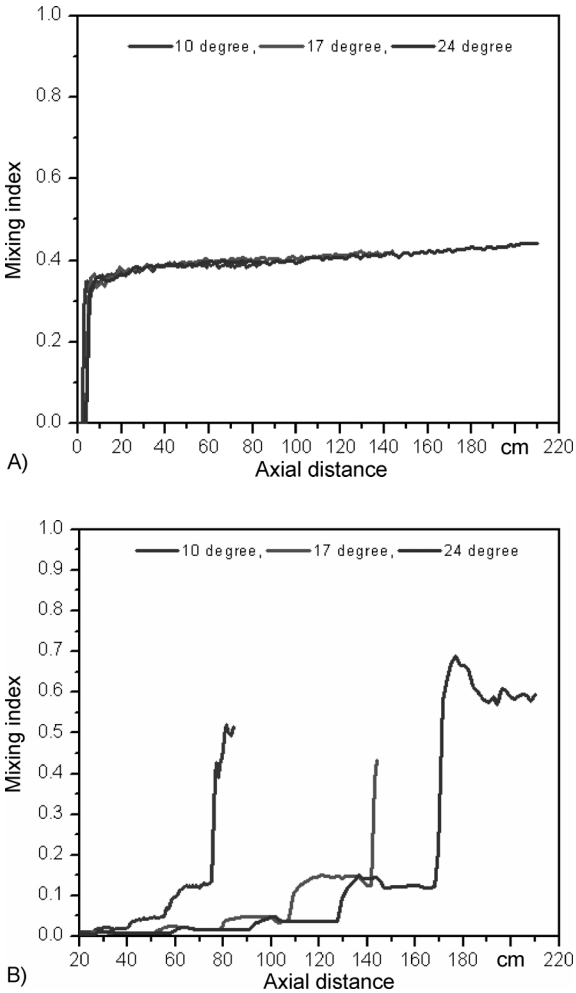

Fig. 10. Evolution of mixing index for the case of the power law fluid, Q_f/Q_d = 0, A: preferred size: 0.011 (smallest), B: preferred size: 0.039 (intermediate)

The weights are positive numbers that must add up to unity:

$$\sum_{c=1}^{C} f_c = 1, \qquad 0 \le f_c \le 1. \tag{13}$$

In the limiting case when only one particular size is important and the others are not, the weight of the favored size is equal to unity and the rest are equal to zero.

In our work we follow the evolution of mixing quality in the single screw extruder with an index defined in Eq. 12 based on Gaussian weights:

$$f_c = A\exp\left[-\frac{(r_c - r_{opt})^2}{2\sigma^2}\right], \qquad A = \left[\sum_{c=1}^{C} \exp\left(-\frac{(r_c - r_{opt})^2}{2\sigma^2}\right)\right]^{-1}. \tag{14}$$

The favored size is r_{opt} and the width of the distribution function is s. The largest weight f is equal to the parameter A which is chosen such as to satisfy the condition expressed in Eq. 13. Note that by increasing the preferred distribution width s, we attribute less significance to the optimum size (smaller value for A).

In this study we consider two case scenarios: one in which the optimum particle size corresponds to the smallest particle size generated during erosion (particles of radius 0.011 cm) and one in which the optimum particle size is arbitrarily chosen at an intermediate size of 0.039 cm. The value of s was chosen to be 0.001286 cm. Fig. 8 shows the weight functions f_c for these two scenarios based on 20 size fractions.

Fig. 9A shows the evolution of the mixing index calculated for three extruder designs operated at a zero throttle ratio in the Newtonian fluid, when the preferred size in the system is the smallest particle size. The fast increase of the index from zero to a value of about 0.35 accounts for the appearance of the smallest size fraction (0.011 cm) in the earliest stages of mixing. The three extruder designs show similar performance in spite of the delayed erosion at higher values of the helix angle. Apparently the dominant factor in this case seems to be the overall distribution process. The small fragments produced from the initial agglomerates tend to move in the fluid close enough to their parents for a long time, thus creating local spots of high particle concentration and impeding on overall mixing quality. On the other hand, when the preferred distribution is shifted to the intermediate particle size, the mixing index is primarily dominated by the concentration of the preferred specie and correlates well with the dispersion kinetics curves. This is illustrated in Fig. 9B.

Similar tendencies are observed when agglomerates dispersion and distribution is taking place within a power law fluid (Fig. 10A and B). In this case however, as the level of dispersion is lower than in the case of a Newtonian fluid, the index indicates less overall mixing efficiency. This is illustrated in Fig. 11 where mixing indices for Newtonian and power law fluids are compared based upon the case of the extruder with 10° helix angle. Other researchers have also reported that shear-thinning behavior of the fluid can result in a decrease in mixing efficiency [26 to 28].

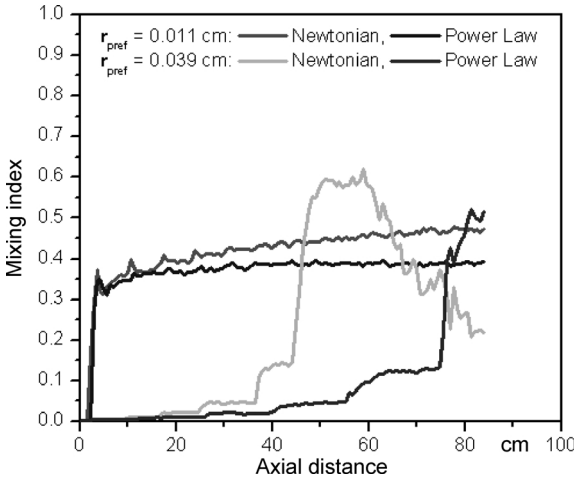

Fig. 11. Comparison between the mixing efficiency of Newtonian and the power law fluids at zero throttle ratio

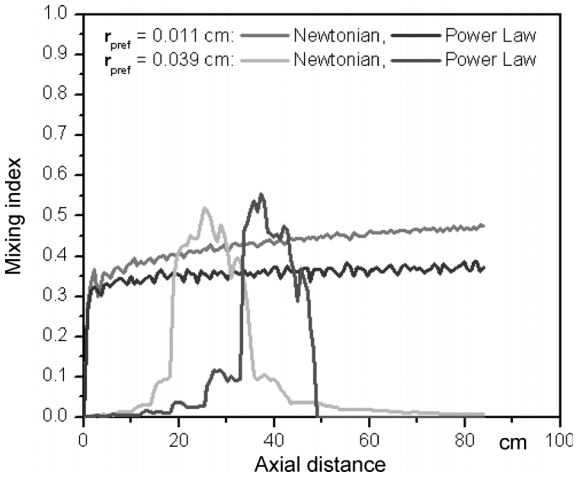

Fig. 13. Comparison between the mixing efficiency of Newtonian and the power law fluids at negative throttle ratio

Similar observations can be made when operating the extruder at a negative throttle ratio as shown in Fig. 12. In general, operating at a negative throttle ratio enhances mixing, both dispersive and distributive. When the preferred size is the smallest one present in the system, a comparison of Fig. 9 and 12 reveals a slight increase in mixing index when operating at negative throttle ratio. Exception to the rule shows the extruder with a helix angle of 10°, for which the mixing index does not change with throttle ratio. For an intermediate preferred size, the maximum in mixing index is shifted early on in the extruder length when operating at a negative throttle ratio. This and the fact that extruders with smaller helix angles show consistently better performance point out to a dominant dispersive mixing effect on the general outcome.

Fluid rheological behavior affects the overall mixing performance with the Newtonian fluid showing better results as illustrated in Fig. 13.

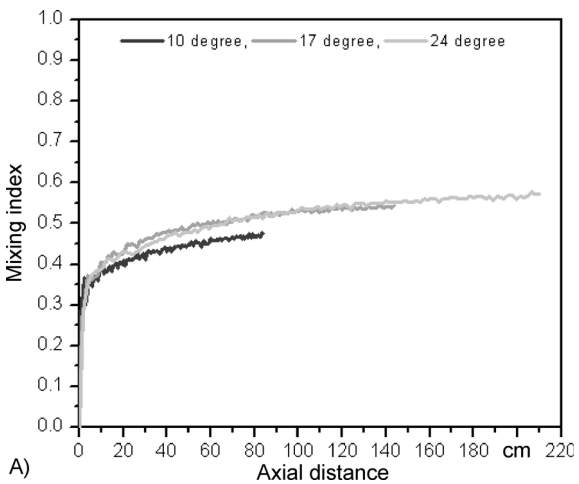

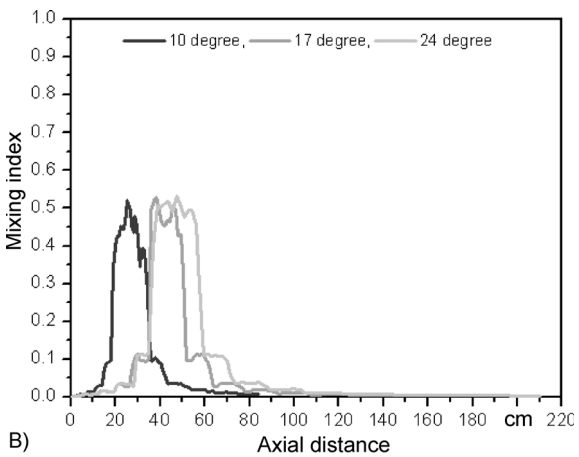

Fig. 12. Evolution of the mixing index along the extruder length when operating the extruder at negative throttle ratio, A: ■, B: ■

5 Conclusions

The Shannon entropy was adapted to quantify mixing processes taking place in a single screw extruder by simultaneously accounting for dispersive and distributive mixing. A mixing index based on a weighted average of the entropies associated with different species present in the system (as defined by particle size) was developed. This index can be tailored to reflect various physical properties of the system as affected by a preferred particle size. The new mixing index has potential to be used for equipment design and process optimization as demonstrated here in the study of the influence of helix angle (design) and throttle ratio (processing conditions) on the evolution of the index along the extruder length.

References

1 *Manas–Zloczower, I., Tadmor, Z.:* Adv. Polym. Tech. 3, p. 213 (1983)
2 *Cheng. J., Manas–Zloczower, I.:* Polym. Eng. Sci. 29, p. 701 (1989)
3 *Gramann, P. J., Osswald, T. A.:* Int. Polym. Process. 3, p. 303 (1992)
4 *Gramann, P. J., Noriega, M. d. P., Rios, A. C., Osswald, T. A.:* SPE Antec Tech Papers, 43, p. 3713 (1997)

IPP_ipp_2004_04_1843 – 17.12.04/druckhaus

5 *Yao, C. H., Manas–Zloczower, I.:* Int. Polym. Process., 2, p. 92 (1997)
6 *Rios, A. C., Gramann, P. J., Osswald, T. A., Noriega, M. d. P., Estrada, O. A.:* Int. Polym. Process. 15, p. 12 (2000)
7 *Rauwendaal, C., Osswald, T. A., Gramann, P., Davis, B.:* Int. Polym. Process. 14, p. 28 (1999)
8 *Ishikawa, T., Amano, T., Kihara, S., Funatsu, K.:* Polym. Eng. Sci. 42, p. 925 (2002)
9 *Yao, W., Mishima, M., Takahashi, K.:* Chem. Eng. J. 84, p. 565 (2001)
10 *Tadmor, Z., Gogos, C. G.:* Principles of Polymer Processing. John Wiley & Sons, New York, Chichester, Brisbane, Toronto, Singapore (1979)
11 *Galaktionov, O. S., Anderson, P. D., Peters, G. W. M., Meijer, H. E. H.:* Int. Polym. Process. 18, p. 138 (2003)
12 *Galaktionov, O. S., Anderson, P. D., Kruijt, P. G. M., Peters, G. W. M., Meijer, H. E. H.:* Comput. Fluids 10, p. 1942 (2001)
13 *Kruijt, P. G. M., Galaktionov, O. S., Anderson, P. D., Peters, G. W. M., Meijer, H. E. H.:* AIChE J. 47, p. 1005 (2001)
14 *Danckwerts, P. V.:* Appl. Sci. Res. A 3, p. 279 (1953)
15 *Yang, H. H., Wong, T., Manas–Zloczower, I.,* in: Mixing and Compounding of Polymers. Manas–Zloczower, I., Tadmor, Z. (Eds.), Hanser Publishers, Munich (1994)
16 *Hutchinson, B. C., Rios, A. C., Osswald, T. A.:* Int. Polym. Process. 14, p. 315 (1999)
17 *Tucker, C. L., Peters, G. W. M.:* Korea-Australia Rheol. J. 15, p. 197 (2003)
18 *Wang, W., Manas–Zloczower, I., Kaufman, M.:* Int. Polym. Process. 16, p. 315 (2001)
19 *Wang, W., Manas–Zloczower, I., Kaufman, M.:* AICHE J. 49, p. 1637 (2003)
20 *Shearer, G., Tzoganakis, C.:* Polym. Eng. Sci. 40, p. 1095 (2000)
21 *Shearer, G., Tzoganakis, C.:* Polym. Eng. Sci. 41, p. 2206 (2001)
22 *Ottino, J. M.:* The Kinematics of Mixing: Stretching, Chaos, and Transport. Cambridge University Press, Cambridge, New York, Port Chester, Melbourne, Sydney (1989)
23 *Shannon, C. E.:* The Bell System Technical J. 27, p. 379 (1948)
24 *Press, W. H., Teukolsky, S. A., Vetterling, W. T., Flannery, B. P.:* Numerical Recipes in Fortran: The Art of Scientific Computing. Cambridge University Press, Cambridge, New York (1992)
25 *Scurati, A., Manas–Zloczower, I., Feke, D. L.:* ACS-Rubber Div. Meeting Proceed. Atlanta, GA (2002)
26 *Niederkorn, T. C., Ottino, J. M.:* AIChE J. 40, p. 1782 (1994)
27 *Ling, F. H., Zhang, X.:* J. Fluids Eng. 117, p. 75 (1995)
28 *Anderson, P. D., Galaktionov, O. S., Peters, G. W. M., van de Vosse, F. N., Meijer, H. E. H.:* J. Non-Newtonian Fluid Mech. 93, p. 265 (2000)

Acknowledgements

The authors would like to acknowledge National Science Foundation for the financial support (Grant number DMI-0140412) and Ohio Supercomputer Center for the use of computing facilities.

Date received: ■
Date accepted: ■

IPP_ipp_2004_04_1843 – 17.12.04/druckhaus